Planetary and Space Science 156 (2018) 2–6

Contents lists available at ScienceDirect

Planetary and Space Science

journal homepage: www.elsevier.com/locate/pss

Nanodust released in interplanetary collisions

H.R. Lai *, C.T. Russell

IGPP/EPSS, UCLA, USA

ARTICLE INFO

Keywords:
Interplanetary collisions
Nanodust
Interplanetary field enhancement

ABSTRACT

The lifecycle of near-Earth objects (NEOs) involves a collisional cascade that produces ever smaller debris ending with nanoscale particles which are removed from the solar system by radiation pressure and electromagnetic effects. It has been proposed that the nanodust clouds released in collisions perturb the background interplanetary magnetic field and create the interplanetary field enhancements (IFEs). Assuming that this IFE formation scenario is actually operating, we calculate the interplanetary collision rate, estimate the total debris mass carried by nanodust, and compare the collision rate with the IFE rate. We find that to release the same amount of nanodust, the collision rate is comparable to the observed IFE rate. Besides quantitatively testing the association between the collisions evolving large objects and giant solar wind structures, such a study can be extended to ranges of smaller scales and to investigate the source of moderate and small solar wind perturbations.

1. Introduction

By June 1 2017, more than 16,000 near-Earth objects (NEOs) have been discovered (https://cneos.jpl.nasa.gov/stats/size.html), and the number of NEOs is expected to increase dramatically as the size of the NEOs decreases (Johnson, 2014).

As Fig. 1 shows, collisional cascade is involved in the lifecycle of the NEOs. It grinds up the NEOs to smaller and smaller debris. The dynamics of the debris are governed by different effects, depending on the debris' sizes. For particles larger than a micrometer in diameter, they will spiral into the Sun under the Poynting-Robertson effect; while the nanoscale particles can be picked up via electromagnetic forces.

The debris released in collisions generally constitutes a large amount in a relatively short time and limited space. Therefore, instead of picking up the nanodust individually, the solar wind interacts with a cloud of nanodust coherently. Such interactions could perturb the background interplanetary magnetic field (IMF) significantly and create a unique magnetic structure called an interplanetary field enhancement (IFE).

IFEs are characterized by a cusp-shaped enhancement in the field strength and strong central current sheets (Russell et al., 1983). It has been proposed that the former signature is caused by the pileup of the magnetic field in the upstream region of the dust cloud, transferring momentum from the solar wind to push the dust away from the Sun (Lai et al., 2013; Lai et al., 2015). Lai et al., (2015) explained the latter signature as the twist of the magnetic field due to the existence of heavy charged particles (Jia et al., 2012). Statistical studies also reveal that solar wind is slowed down in the upstream region of the dust cloud (Lai et al., 2013).

IFEs as collisional signatures have been used to identify co-orbiting objects of known NEOs (Russell et al., 1984; Lai et al., 2017). Those co-orbitals may be generated in early collisions and are still subject to continuous collisions. This new survey technique is powerful as it is sensitive to small objects which are otherwise "invisible" to a traditional terrestrial-based optical telescope. In addition, most of the interplanetary spacecraft are equipped with magnetometers, and their data can be used in such a technique.

Although early studies have already qualitatively tested the relation between IFEs and collisions, the quantitative comparison between the IFE rate and collision rate is still elusive. To further test this IFE formation scenario, we compare an estimated interplanetary collision rate to the IFE rate in this paper. In Section 2, we review the statistical properties of IFEs detected at 1AU, including their annual rate, scale and the mass of related dust clouds. In Section 3, we introduce our model calculating the interplanetary collision rate and compare the modeled results with IFE observations. Section 4 summarizes this study.

2. IFE properties

One-Hz magnetic field data from the Advanced Composition Explorer (ACE) (Smith et al., 1998) are used to survey the IFEs at 1AU. We use the same IFE selection criteria (Lai et al., 2013; Lai et al., 2014; Lai et al., 2017): (1) the magnetic field enhancement $\frac{B_{max}-B_{amb}}{B_{amb}}$ is at least 25%; (2)

* Corresponding author.
E-mail address: hlai@igpp.ucla.edu (H.R. Lai).

https://doi.org/10.1016/j.pss.2017.10.003
Received 15 June 2017; Received in revised form 11 September 2017; Accepted 9 October 2017
Available online 10 October 2017
0032-0633/© 2017 Elsevier Ltd. All rights reserved.

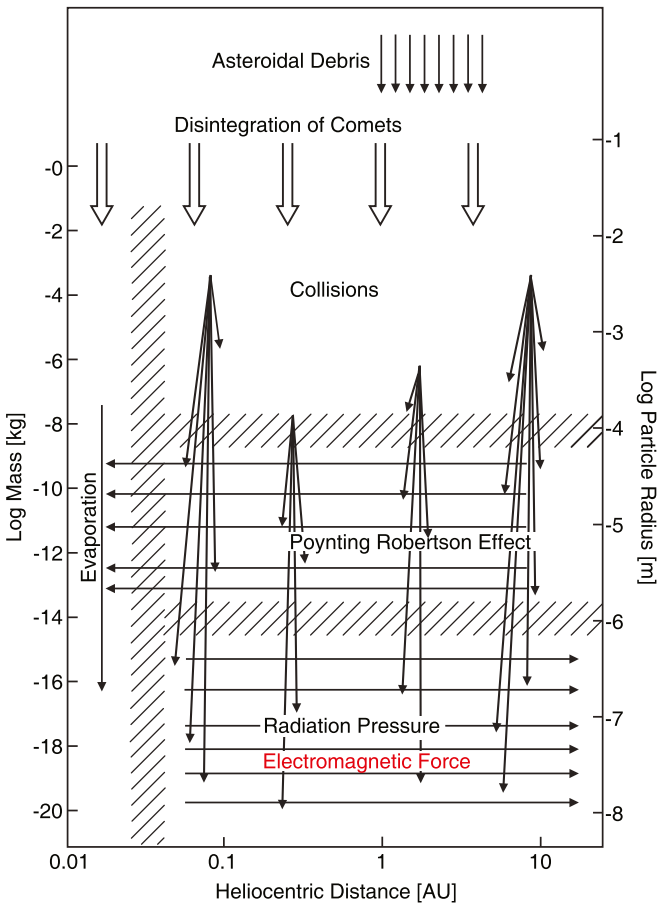

Fig. 1. The collisional cascade that grinds meteoroids and asteroids into dust, which falls into the Sun or is blown out of the solar system (after Grün et al., 1985).

the influence period (see Fig. 2) of the IFEs is at least 10 min; (3) no smooth rotation is shown in the magnetic field during the event. An example of moderately large IFEs is shown in Fig. 2.

In total, 103 IFEs are identified from 1998 to 2011. Since the IFEs generally move at nearly the solar wind speed (e.g., Russell et al., 2010; Lai et al., 2015), the radial scale of the IFEs is defined as the product of the solar wind speed and the event duration. Here the solar wind speed is measured by solar wind electron proton alpha monitor (SWEPAM) on ACE (McComas et al., 1998). Fig. 3a shows the IFE annual rate binned by the radial scale.

To estimate the mass of the dust cloud contained in the IFEs, Lai et al., (2014) calculate the gradient force on the IFEs by integrating the pressure difference over the IFE cross section, which is proportional to the square of the radial scale. Lai et al., (2015) confirm that this force is consistent with the solar wind slowdown. By balancing the pressure gradient force with the solar gravity, the mass contained in the IFEs is estimated (e.g., Lai et al., 2014; Lai et al., 2017). We use the same technique here, and the mass distribution is shown in Fig. 3b. We note that the IFE rate is a non-monotonic function of the mass. Due to the selection criteria, we might have undercounted the very weak and small IFEs, as shown in the left-most bar in Fig. 3b. In addition, there are few very large IFEs. Therefore, the right-most bars in Fig. 3a and b have less statistical accuracy.

3. Collision model and results

3.1. Interplanetary collision model

As calculated by Grün et al., (1985), the impactors (the smaller objects in these binary collisions) can disrupt targets (the larger objects in the collisions) 10^6 times larger than themselves in mass when the collisional speed is tens of kilometers per second. Thus we must investigate the interplanetary objects over a wide range of masses. Below we modify the influx model given by Ceplecha (1992) to obtain the interplanetary flux model at 1AU.

Ceplecha (1992) employed observations in different mass ranges and reconstructed the flux of the interplanetary objects from 10^{-20}kg to 10^{15}kg coming to the entire surface of the Earth. To convert this influx model to a more general interplanetary flux model, we scale Ceplecha's model so that it matches the lunar flux model (Grün et al., 1985) from 10^{-20}kg to 10^{-10}kg, as shown in Fig. 4a. The differential spatial number density at 1AU is then $\frac{dN(m,r_0)}{d(\log_{10}m)} = \frac{dF(m,r_0)}{d(\log_{10}m)}\frac{k}{V(r_0)}$. Here F is the cumulative flux, N is the cumulative spatial density, r_0 is 1AU and $k = 4$ in the case of an isotropic flux. $V(r)$ is the average collisional velocity and $V(r) = V_0\left(\frac{r}{r_0}\right)^{0.5}$ with $V_0 = 20$km/s (Grün et al., 1985). Inside 1AU, we assume that the number density of the interplanetary bodies is $\left(\frac{r}{r_0}\right)^{-1.5}$ (Leinert et al., 1978).

Here we consider catastrophic collisions only, which are defined in situations when the largest fragment contains at most 50% of the target's mass. Such collisions are expected to produce nanoscale dust most efficiently. Catastrophic collisions happen when the mass ratio between the target (m_1) and the impactor (m_2) satisfies $\frac{m_1}{m_2} \le T$, where T is a function of the collisional speed and the material properties of the targets. We use the same model as Grün's $T(r) = T_0\left(\frac{r}{r_0}\right)^{-1}$, where $T_0 = 9.76\times10^2 S_c^{-0.45}\left(\frac{m_1}{\rho_1}\times10^6\right)^{0.075} v_0^2$. For a crystalline rock target, $S_c = 3$kbar and $\rho_1 = 2.5\times10^3$kg. Fig. 4b shows estimated T_0 as a function of the target mass at 1AU. We can see that when the collisional velocity is 20 km/s, T is generally larger than 10^4 and can reach 10^6 when the mass of the target is larger than 5.13×10^5kg.

The collisional cross section can be expressed as $\sigma(m_1,m_2) = \pi\left(\frac{3}{4\pi\rho}\right)^{\frac{2}{3}}\left(m_1^{\frac{1}{3}}+m_2^{\frac{1}{3}}\right)^2$ and the rate of catastrophic collisions of a target (m_1) by impactors (m_2) in the range $m_1/T \le m_2 < M_\infty$ is given by

$$-\int_{m_1/T}^{M_\infty}\sigma(m_1,m_2)k\frac{dF(m_2,r)}{d(\log_{10}m_2)}d(\log_{10}m_2). \quad (1)$$

In a unit volume, the collision rate between targets (m_1) and impactors (m_2) is thus

$$\frac{dN(m_1,r)}{d(\log_{10}m_1)}\int_{m_1/T}^{M_\infty}\sigma(m_1,m_2)k\frac{dF(m_2,r)}{d(\log_{10}m_2)}d(\log_{10}m_2).$$

Here M_∞ is set to be 10^{15}kg and the negative sign in (1) is due to the definition of cumulative flux.

After collision, the mass of the targets and impactors is carried by the debris. To get the debris distribution, we extrapolate the experimental results of Fujiwara et al., (1977) to small debris regions and assume that the mass distribution of the fragments can be approximated by a power law (Grün et al., 1985)

$$\frac{dG(m,m_1,m_2)}{d(\log_{10}m)} = c_1 m^{-\eta}.$$

Here $\eta = 0.83$ and c_1 can be calculated from the conservation of mass

$$\int_0^{m_L} m\frac{dG(m,m_1,m_2)}{d(\log_{10}m)}d(\log_{10}m) = m_1.$$

The mass of the largest fragment m_L is found to be

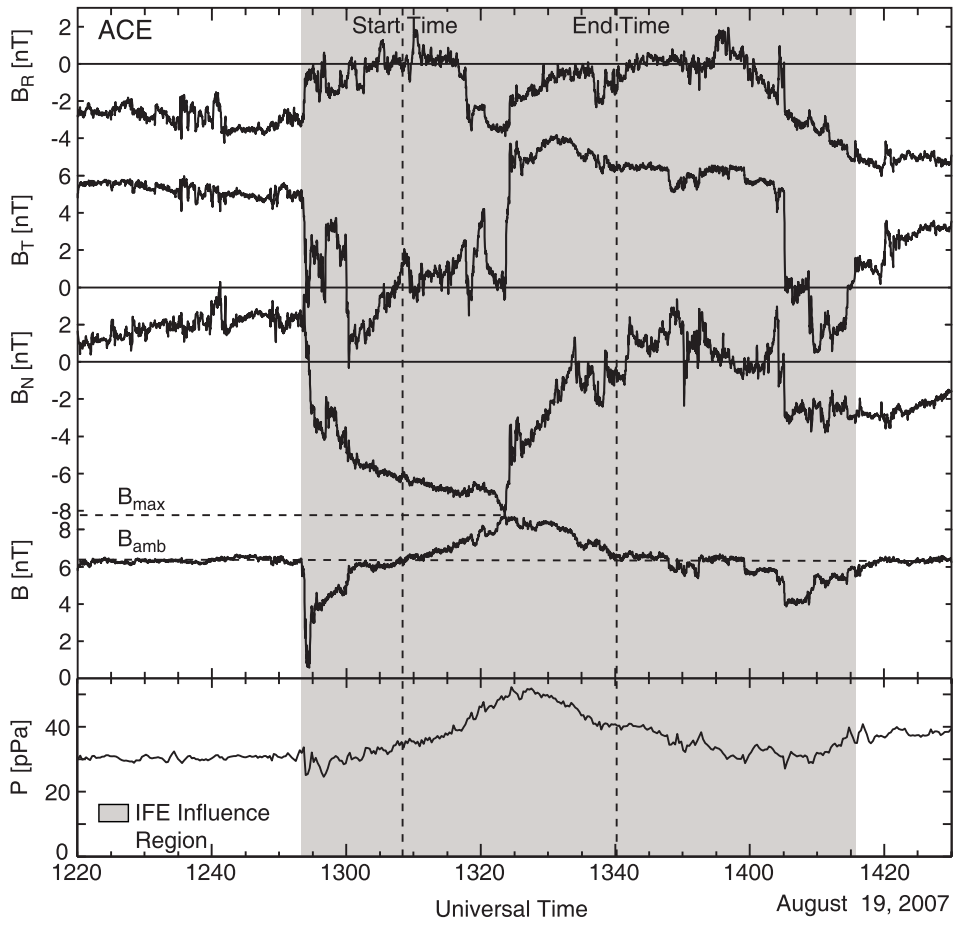

Fig. 2. An IFE example illustrating the definition of magnetic field enhancement, duration, and influence period. The magnetic field components are in radial, tangential, and normal coordinate system. The bottom panel shows the sum of the magnetic and plasma thermal pressure.

$$\frac{m_L}{m_1} \approx 9.26 \times 10^{-8} \left(\frac{m_2}{m_1}\right)^{-1.24} \cdot \left(\frac{r}{r_0}\right)^{1.24}.$$

If the IFE signature is associated with the pickup of collisional debris, we are interested in the mass carried by nanoscale particles. We assume that the maximum mass of the dust particle is m'; the total mass of the dust cloud is then

$$\int_0^{m'} m \frac{dG(m, m_1, m_2)}{d(\log_{10} m)} d(\log_{10} m).$$

We insert the numbers and get the expression for the mass of the dust cloud produced by a collision between m_1 and m_2.

$$m_d = 15.6919 m'^{0.17} m_1^{0.6192} m_2^{0.2108} \left(\frac{r}{r_0}\right)^{-0.2108}.$$

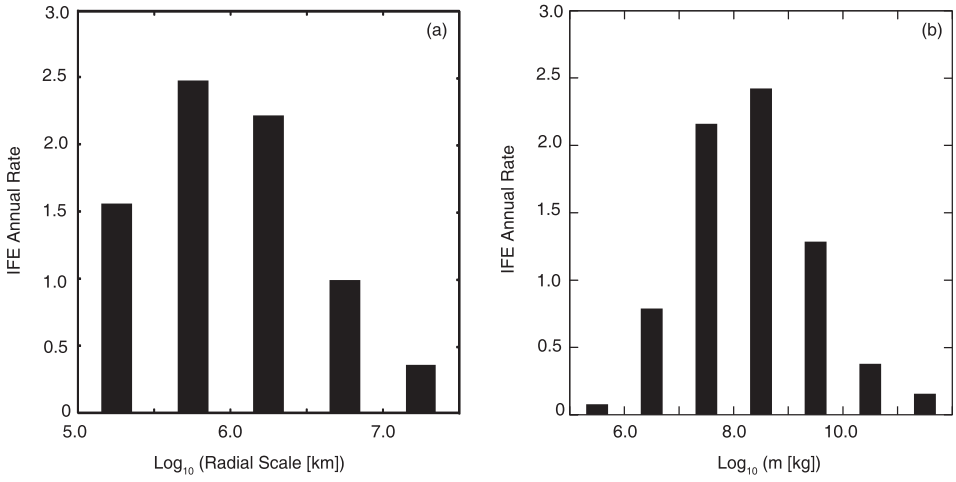

Fig. 3. (a) IFE annual rate as a function of radial scale. (b) IFE annual rate as a function of estimated mass.

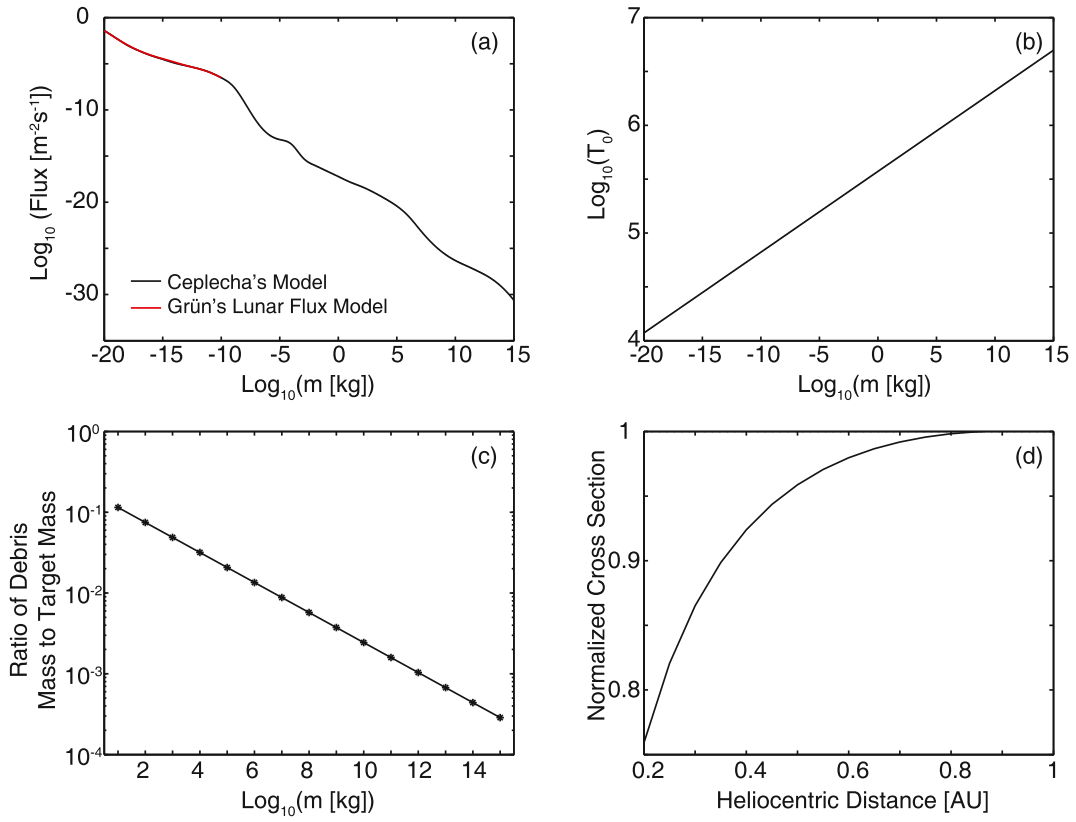

Fig. 4. (a) Flux model of the interplanetary objects modified from Ceplecha (1992). (b) T_0 is the mass ratio of a target to the smallest impactor that can catastrophically destroy the target. (c) Ratio of debris mass (up to 500 nm in diameter) to the mass of target as a function of the target mass. (d) The heliocentric radial variation of the IFE cross section normalized to the one at 1AU.

Fig. 4c shows the ratio of debris mass carried by dust with diameters of up to 500 nm to the mass of the targets at 1AU. Here we only consider the collisions that can barely destroy the target disruptively, thus the impactor is one T_0 times smaller in mass. From Fig. 4c we can see that the debris released by smaller objects is generally in smaller sizes.

In equation (1), as we integrate m_2 to 10^{15}kg, we expect that when $m_1 \geq \frac{m_2}{T}$, m_2 can also be catastrophically destroyed. Therefore in our debris distribution model, we consider the total mass of the nanoscale debris.

With the above knowledge, we can estimate the collision rate as a function of the mass carried by nanoscale particles. However, this is not the counterpart of the IFE rate. Since the IFEs, after they are formed and before they dissipate, are carried outward by the solar wind and are expected to be detected by the spacecraft which pass by, the counterpart of the IFE annual rate is the cumulative collision rate in a certain production volume.

We adopt a simple model of the production volume by assuming that it starts at 0.2AU, inside of which nanoscale dust particles will be lost due to evaporation (Czechowski and Mann, 2010, 2011). We also assume that the IFE mass does not change during its anti-sunward travel. Therefore, the radial variation of the IFE cross section is given by

$$\frac{A}{A_0} = \frac{\left(\frac{B_0^2}{2\mu_0} + N_0 k T_0\right) r_0^2}{\left(\frac{B^2}{2\mu_0} + NkT\right) r^2}.$$

Here A is the cross section of the IFEs, r is the heliocentric distance, N is the solar-wind proton number density, T is the sum of proton (T_p) and electron (T_e) temperatures and the symbols with subscript zero (except μ_0) are the values at 1AU. T_e is set to be a constant of 130000 K. The radial variations of the field strength, proton number density and temperature are from Köhnlein (1996).

$$\log_{10} B = 0.5 - 1.1 \log_{10} r + 0.2815 e^{0.875 \log_{10} r}$$

$$\log_{10} N = 0.7766 - 1.934 \log_{10} r + 0.01823 e^{-2.245 \log_{10} r}$$

$$\log_{10} T_p = 4.858 - 0.668 \log_{10} r$$

The calculated normalized cross section is shown in Fig. 4d. We can see that the cross section of IFEs expands slowly as they move outward. Therefore, the production volume is a truncated cone starting from 0.2AU.

3.2. IFE rate vs. collision rate at 1AU

By integrating the collision rate inside the production volume and assuming all debris clouds remain detectable by their magnetic disturbance, we can estimate the expected detectable collision rate at 1AU. We alter the maximum dust size and show the results in Fig. 5. The IFE rate based on ACE is also plotted to make a comparison. The mass range here is from 10^6kg to 10^{10}kg where the IFE results are best defined statistically. We find that the differences between the IFE rate and the collision rates corresponding to an upper limit dust size of 150 nm are always within an order of magnitude. In addition, the non-monotonic variation is reproduced. This can be explained by a compromise between the production volume and the collision rate. The former increases with the mass due to the increasing IFE cross section, while the latter decreases with the mass as there are few larger interplanetary objects.

4. Conclusion and discussion

In this paper, we modify the influx model of Ceplecha (1992) and the collision model of Grün (et al., 1985) to estimate the interplanetary collision rate. To compare these models with the IFE rate, we assume that

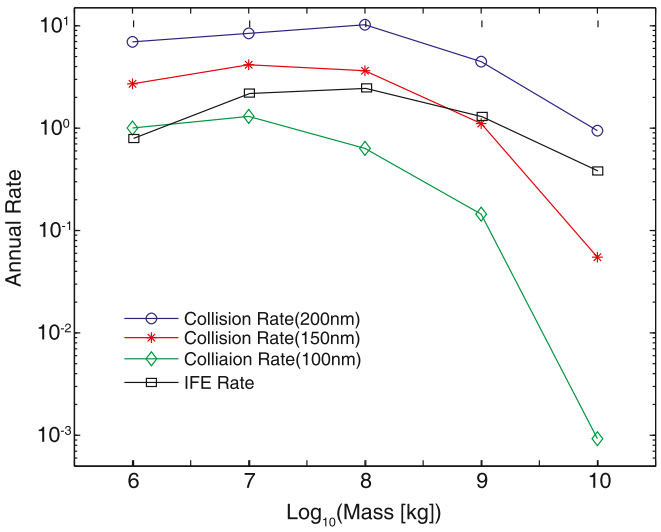

Fig. 5. Calculated detectable collision rate compared with the observed IFE rate at 1AU.

the volume in which these collisionally produced dust clouds can later be detected is a truncated cone starting at 0.2AU with a cross section expanding as the heliocentric distance increases. At 1AU, we find that the expected collisions in the volume are comparable with the observed IFE rate.

The IFE mass calculation model and the collisional model used in this study are simple. However, the results are in surprisingly good agreement. The key improvements of the IFE mass estimation are to determine the force on the IFE more accurately and determine the acceleration of the IFEs. With well-spaced multi-spacecraft simultaneous observations, the force on the IFEs can be determined more accurately (Lai et al., 2015). As we now have one more spacecraft, DSCOVR, providing magnetic and plasma data at the first Lagrangian point, we should soon have more multi-spacecraft observations of the IFEs. However, even with multi-spacecraft observations, the acceleration of the IFEs is still hard to measure. A good way to obtain this property is to use the numerical models, which can reproduce the IFEs from birth to death. The multi-fluid model in Jia et al., (2012) has studied a similar situation when a magnetized plasma flow passes a charged dust flow. In the initial stage of the interaction, the resulting magnetic signatures are qualitatively similar to the observed IFEs. A more ideal case is to put a cloud of charged dust in a magnetized plasma flow and track the entire evolution of both the dust cloud and the background plasma.

The collision rate calculation model can be improved in many ways: a more updated interplanetary flux model from observation, a more accurate catastrophic collision model and debris distribution model from experiments, and a better determined model of production volume. The last one can be obtained again from numerical simulations. As the IFEs evolve, we expect the dust cloud to expand and the magnetic structure to dissipate. The lifetime of the IFEs would be even more important if we were to compare the collision rate with the IFE rate detected by Ulysses (Jones et al., 2003), which went out up to 5.5AU. An event list and an atlas of the magnetic field profiles are included in Jones's paper, which help in deriving the IFE rate and mass of the dust clouds there.

In this study, we focus on the collisions evolving relatively large objects to quantitatively compare their collision rate with the IFE rate. However, collisions between small objects also affect the solar wind as long as there are electromagnetic interactions. The resultant IMF structures may be too small or too weak to be classified as IFEs, but their geometry can be predicted in the same solar wind-dust cloud interaction simulation. An extended application of our collision model is to calculate the collision rate in the smaller size range and convert the results to be the rate as a function of the typical size of the IMF structures. This can then be compared with the solar wind and interplanetary field observations. Such a comparison may be relevant to the production of turbulence in the solar wind flow (e.g., Tu and Marsch 1995) and the observation of plasma jets in the magnetosheath (e.g., Němeček et al., 1998) with enhanced interplanetary momentum flux.

References

Ceplecha, Z., 1992. Influx of interplanetary bodies onto Earth. Astron. Astrophys. 263, 361–366.

Czechowski, A., Mann, I., 2010. Formation and acceleration of nano dust in the inner heliosphere. Astrophys. J. 714, 89–99.

Czechowski, A., Mann, I., 2011. Erratum: formation and acceleration of nano dust in the inner heliosphere. Astrophys. J. 732, 127, 127.

Fujiwara, A., Kamimoto, G., Tsukamoto, A., 1977. Destruction of basaltic bodies by high-velocity impact. Icarus 31, 277–288.

Grün, E., Zook, H.A., Fechtig, H., Giese, R.H., 1985. Collisional balance of the meteoritic complex. Icarus 62, 244–272.

Jia, Y.D., Ma, Y.J., Russell, C.T., Lai, H.R., Toth, G., Gombosi, T.I., 2012. Perpendicular flow deviation in a magnetized counter-streaming plasma. Icarus 218, 895–905.

Johnson, L., 2014. Finding Near Earth Objects before They Find Us. In: Asteroid Grand Challenge: Virtual Seminar Series. http://sservi.nasa.gov/wp-content/uploads/2014/02/NASA-NEO-Program-AGC-Seminar.pdf.

Jones, G., Balogh, A., McComas, D.J., MacDowall, R.J., 2003. Strong interplanetary interplanetary field enhancements at Ulysses—evidence of dust trails' interaction with the solar wind? Icarus 166, 297–310.

Köhnlein, W., 1996. Radial dependence of solar wind parameters in the ecliptic (-61AU). Sol. Phys. 169, 209–213.

Lai, H.R., Wei, H.Y., Russell, C.T., 2013. Solar wind plasma profiles during interplanetary field enhancements (IFEs): consistent with charged-dust pickup. AIP Conf. Proc. 1539, 402–405.

Lai, H.R., Russell, C.T., Wei, H.Y., Zhang, T.L., 2014. The evolution of co-orbiting material in the orbit of 2201 Oljato from 1980 to 2012 as deduced from Pioneer Venus Orbiter and Venus Express magnetic records. Meteorit. Planet. Sci. 49, 28–35.

Lai, H.R., Russell, C.T., Jia, Y.D., Wei, H.Y., Angelopoulos, V., 2015. Momentum transfer from solar wind to interplanetary field enhancements inferred from magnetic field draping signatures. Geophys. Res. Lett. 42 https://doi.org/10.1002/2015GL063302.

Lai, H.R., Russell, C.T., Wei, H.Y., Connors, M., Delzanno, G.L., 2017. Possible potentially threatening co-orbiting material of asteroid 2000EE104 identified through interplanetary magnetic field disturbances. Meteorit. Planet. Sci. 1–8. https://doi.org/10.1111/maps.12854.

Leinert, C., Hanner, M., Pitz, E., 1978. On the spatial distribution of interplanetary dust near 1AU. Astron. Astrophys. 63, 183–187.

McComas, D.J., Bame, S.J., Barker, P., Feldman, W.C., Phillips, J.L., Riley, P., Griffee, J.W., 1998. Solar wind electron proton alpha monitor (SWEPAM) for the advanced composition explorer. Space Sci. Rev. 86, 563–612.

Němeček, Z., Šafránková, J., Přech, L., Sibeck, D.G., Kokubun, S., Mukai, T., 1998. Transient flux enhancements in the magnetosheath. Geophys. Res. Lett. 25, 1273–1276. https://doi.org/10.1029/98GL50873.

Russell, C.T., Luhmann, J.G., Barnes, A., Mihalov, J.D., Elphic, R.C., 1983. An unusual interplanetary event: encounter with a comet? Nature 305, 612–615.

Russell, C.T., Aroian, R., Arghavani, M., Nock, K., 1984. Interplanetary magnetic field enhancements and their association with the asteroid 2201 Oljato. Science 226, 43–45.

Russell, C.T., Weimer, D.R., Omidi, N., Jian, L.K., Luhmann, J.G., Strangeway, R.J., 2010. Interplanetary field enhancements travel at the solar wind speed. Geophys. Res. Lett. 37, L07204 https://doi.org/10.1029/2010GL042618.

Smith, C.W., L'Heureux, J., Ness, N.F., Acuña, M.H., Burlaga, L.F., Scheifele, J., 1998. The ACE magnetic fields experiment. Space Sci. Rev. 86, 613–632.

Tu, C.Y., Marsch, E., 1995. MHD structures, waves and turbulence in the solar wind: observations and theories. Space Sci. Rev. 73, 1–210.